9.2 HOW CAN WE DESCRIBE THE ENTRAINMENT PROCESSES IN SHEARED CONVECTIVE BOUNDARY LAYERS?: A LARGE–EDDY SIMULATION AND MIXED–LAYER THEORY/MODEL COMPARISON STUDY

David Pino *
Applied Physics Department, Technical University of Catalonia, and
Institute for Space Studies of Catalonia (IEEC/CSIC), Barcelona, Spain
Jordi Vilà-Guerau de Arellano
Meteorology and Air Quality Section, Wageningen University, Wageningen, The Netherlands
Si-Wan Kim
NOAA/ESRL and CIRES, Boulder, CO, USA

1. INTRODUCTION

The description of the heat flux at the interface between the atmospheric boundary layer and the free troposphere is still crudely represented in large atmospheric and chemistry models. In particular, the entrainment of warm and dry air is a crucial process in the growth of the convective boundary layer (CBL). This process depends closely on the different physical contributions to the turbulent kinetic energy (TKE) at the interface. In representing these fluxes at the entrainment zone in large scale atmospheric models, it is advisable to include the most relevant processes, but in addition to consider a simplified description of them.

In spite of its simplicity, the mixed layer, or slab, model (MXL), which assumes a homogeneous and instantaneous distribution of the state variables in the mixed layer below the inversion (Lilly 1968; Stull 1976a, b; Tennekes 1973; Betts 1973; Mahrt and Lenschow 1976), retains the main characteristics of the CBL, and accurately represents its growth.

In this study, two representations of the entrainment processes are used in the MXL. The main difference in the assumptions of these parameterizations is based on the definition of the entrainment zone depth, δ. The most basic approach, proposed first by Lilly (1968), represents the entrainment zone as a sharp discontinuous inversion, ($\delta = 0$), namely a zeroth–order jump model (ZOJ). From the 1970s onwards, and with different degrees of complexity, this approach has been widely applied to study different convective boundary layers applied to problems in atmospheric physics and chemistry.

The interface layer can also be described in a parametric form by a more realistic assumption. Consequently, the entrainment region is assumed to have a finite thickness ($\delta \neq 0$), the so–called first–order jump model (FOJ). An additional requirement in this description is the estimation of the inversion layer thickness (Mahrt and Lenschow 1976).

In the MXL, regardless of the representation of the inversion layer ($\delta = 0$ or $\delta \neq 0$), the equations for heat, moisture and momentum require an additional assumption to solve the closure problem (Stull 1988; Garratt 1992). Due to the key role played by the heat introduced across the inversion zone in the CBL development, the heat flux in the interface zone is usually prescribed in order to solve this closure problem. Therefore, it is assumed that the entrainment heat flux is a fraction of the surface heat flux, $\overline{w\theta_v}|_e = -\beta\overline{w\theta_v}|_s$. Previous research studies (Zeman and Tennekes 1977; Tennekes and Driedonks 1981; Lilly 2002b; Pino et al. 2003; Sorbjan 2004) have directed their efforts towards developing a suitable parameterization of this ratio. These representations include, in addition to the loss of turbulent kinetic energy by the buoyancy process, the production of TKE by the presence of wind shear, and other contributions to the TKE budget.

By using LES data as a verification reference, we investigate the ability of a mixed layer model, using two different approaches (ZOJ and FOJ) and closure assumptions for the TKE at the entrainment zone, to reproduce the main characteristics of the evolution of a well–developed CBL. Several CBL characterized by different conditions of shear on the surface and at the interface, and different inversion strengths are understudy. The two closure assumptions are obtained from the TKE budget by using scaling arguments. To our knowledge, this is the first time that zeroth– and first–order mixed layer approaches incorporating parameterizations of β, which include the shear contribution at the interface, have been tested and compared against LES.

2. NUMERICAL MODELS SETUP

2.1 *Mixed layer model*

Mixed layer theory assumes a uniform distribution of the atmospheric variables through the boundary layer. By integrating the mean equations for the the horizontally averaged averaged values of the virtual potential temperature (Θ_v), and the two velocity components (U, V) with respect to height, z, through the whole planetary boundary layer, the time evolution of the mean values of Θ_v, U, and V in the mixed layer (Θ_{vm}, U_m, and V_m, respectively) are obtained (Garratt 1992):

* *Corresponding author address:* David Pino, Applied Physics Department, Technical University of Catalonia, Avd. del Canal Olímpic s/n, 08860 Castelldefels, Spain; e-mail: david@fa.upc.edu.

$$
\begin{aligned}
\frac{\partial \Theta_{vm}}{\partial t} &= h_1^{-1}\left(\overline{w\theta_v}|_s - \overline{w\theta_v}|_{h_1}\right),\\
\Delta\Theta_v \frac{\partial h_1}{\partial t} &= \delta \frac{\partial\left[\Theta_{vm} + 0.5\Delta\Theta_v\right]}{\partial t} - \overline{w\theta_v}|_{h_1},\\
\frac{\partial \Delta\Theta_v}{\partial t} &= \gamma_\theta \frac{\partial h_1}{\partial t} - \frac{\partial \Theta_{vm}}{\partial t},\\
\frac{\partial U_m}{\partial t} &= -f\Delta V + h_1^{-1}\left(\overline{wu}|_s - \overline{wu}|_{h_1}\right),\\
\Delta U \frac{\partial h_1}{\partial t} &= \delta \frac{\partial\left[U_m + 0.5\Delta U\right]}{\partial t} - \overline{wu}|_{h_1} + 0.5 f\delta\Delta V,\\
\frac{\partial \Delta U}{\partial t} &= \gamma_u \frac{\partial h_1}{\partial t} - \frac{\partial U_m}{\partial t},\\
\frac{\partial V_m}{\partial t} &= f\Delta U + h_1^{-1}\left(\overline{wv}|_s - \overline{wv}|_{h_1}\right),\\
\Delta V \frac{\partial h_1}{\partial t} &= \delta \frac{\partial\left[V_m + 0.5\Delta V\right]}{\partial t} - \overline{wv}|_{h_1} - 0.5 f\delta\Delta U,\\
\frac{\partial \Delta V}{\partial t} &= \gamma_v \frac{\partial h_1}{\partial t} - \frac{\partial V_m}{\partial t},
\end{aligned}
$$

where f is the Coriolis parameter, h_1 is mixed layer depth, γ_θ is the temperature lapse rate in the free troposphere, w is the vertical velocity, capital letters represent horizontal averaged variables, and lower case letters the fluctuating parts. $\Delta\Theta_v$, $\Delta U = U_{gs} + \gamma_u h_1 - U_m$, and $\Delta V = V_{gs} + \gamma_v h_1 - V_m$, are the jumps of the virtual potential temperature and of the horizontal velocities at the inversion, where U_{gs} and V_{gs} are the characteristic values of the two components of the geostrophic velocity in the mixed layer, and γ_u, γ_v are the vertical gradients of these components in the free troposphere. $\overline{w\theta_v}|_s$, $\overline{wu}|_s$, $\overline{wv}|_s$, $\overline{w\theta_v}|_{h_1}$, $\overline{wu}|_{h_1}$, $\overline{wv}|_{h_1}$, are the horizontally averaged heat and momentum fluxes on the surface and at h_1 respectively. Notice that the zeroth–order jump model equations (Tennekes and Driedonks 1981) are retrieved by prescribing $\delta = 0$ in the above equations.

The above equations have more unknown variables than available equations. In order to close the equation set, the entrainment heat flux is usually assumed to be a function of the other mixed layer variables. Additionally, in the case of FOJ the inversion layer thickness needs to be calculated (Mahrt and Lenschow 1976; Deardorff et al. 1980; Kim et al. 2006).

For the ZOJ used here, the parameterization obtained using the local approach of the TKE budget reads (Pino et al. 2003):

$$
\beta_{ZOJ} = C_F\left[1 + \eta^3\left(\frac{u_*}{w_*}\right)^3\right]\frac{1}{1 + C_T/Ri_t - C_M/Ri_{GS}}, \tag{1}
$$

where $C_F = 0.2$, $\eta = 2$, $C_T = 5$ and $C_M = 0.7$, and Ri_t, Ri_{GS} are two bulk Richardson numbers defined as:

$$
Ri_t = \frac{g h_1}{\Theta_{vm}}\frac{\Delta\Theta_v}{\sigma_m^2}, \quad Ri_{GS} = \frac{g h_1}{\Theta_{vm}}\frac{\Delta\Theta_v}{(\Delta V_e)^2},
$$

where $\sigma_m = \left(w_*^3 + \eta^3 u_*^3\right)^{1/3}$ is a characteristic turbulent velocity, u_* and w_* are the friction and convective velocities, and $(\Delta V_e)^2 = (\Delta U)^2 + (\Delta V)^2$ is the modulus of the velocity inversion jump.

The FOJ used in our study parameterizes the entrainment flux ratio based on the TKE budget integration (Kim et al. 2006). The expression reads:

$$
\begin{aligned}
\beta_{FOJ} = &\left[1 - \frac{\Theta_{vm}(\Delta V_e)^2}{2g(\Delta\Theta_v - 0.5\gamma_\theta\delta)(h_1+\delta)}A_3\right]^{-1}\\
&\left\{A_1\frac{1}{1+\delta/h_1} + A_2\left(\frac{u_*}{w_*'}\right)^3 + A_3\frac{\delta}{4h_1+2\delta}\right.\\
&\left.\left[\frac{u_*^2\Delta V_e}{w_*'^3} + \frac{\Theta_{vm}(\Delta V_e)^2}{g\,(h_1+\delta)\,(\Delta\Theta_v - 0.5\gamma_\theta\delta)}\right]\right\},
\end{aligned} \tag{2}
$$

where $w_*'^3 = g\overline{w\theta_v}|_s(h_1+\delta)/\Theta_{vm}$, and $A_1 = 0.2$, $A_2 = 0.26$, and $A_3 = 1.44$ are constants. The other symbols have the same meaning as in (1). Expression (2) slightly differs from to the one described by Kim et al. (2006). There, the characteristic velocity scale at the inversion was defined as $\Delta\hat{U} = 0.5\left(|\Delta U| + |\Delta V|\right)$. In our research, by using the same $\Delta V_e = \left[(\Delta U)^2 + (\Delta V)^2\right]^{0.5}$ in both ZOJ and FOJ approaches we prescribe the same velocity scaling at the inversion and the same initial condition for the modeling intercomparison. By so doing, we focus the discussion on the contributions of the different terms of the TKE equation on both approaches. In addition, we can retrieve ZOJ parameterization from FOJ by imposing $\delta = 0$.

Additionally, the inversion layer thickness needs to be calculated in the case of FOJ (Mahrt and Lenschow 1976; Deardorff et al. 1980; Kim et al. 2006). The diagnostic equation used to calculate δ was derived in Kim et al. (2006). By using a parcel method, and taking into account the influence of the shear and temperature jump at the inversion, this equation reads:

$$
\delta = h_1\left(aRi^{-1} + b\right), \tag{3}
$$

where $a = 1.12$, $b = 0.08$ have been obtained by a least squares quadratic fit, and Ri is a Richardson number defined as:

$$
Ri = \frac{g h_1}{\Theta_{vm}}\frac{\Delta\Theta_v}{w_\delta^2},
$$

with $w_\delta^2 = w_*^2 + 4u_*^2 + 0.1(\Delta U^2 + \Delta V^2)$.

2.2 *LES setup*

The LES model is described by Cuijpers and Duynkerke (1993), and was lately modified by Cuijpers and Holtslag (1998). The domain is a $10 \times 10 \times 2.032$ km^3 discretized by $256 \times 256 \times 64$ points in each direction. We considered two different sheared CBLs by prescribing a constant on time surface virtual potential temperature flux equal to 0.1 K m s^{-1}, shear forcing (constant geostrophic wind of $U_g = 20$ m s^{-1}, $V_g = 0$ m s^{-1} in the whole domain), but different thermal stratification in the free atmosphere above the mixed layer:

- Case W (weak): temperature lapse rate $\gamma_{\theta(w)} = 0.003$ K m^{-1}, which produces a CBL with a weak capping inversion.

- Case S (strong): with a temperature lapse rate equal to $\gamma_{\theta(s)} = 0.006$ K m^{-1}, which results in a CBL with a strong capping inversion.

For each case, the prescribed initial virtual potential temperature changes vertically from its surface value (300 K) at a constant rate of $\gamma_{\theta(w)}$ and $\gamma_{\theta(s)}$ respectively.

In the two cases, the initial mean wind is $U = 20$ m s^{-1}, $V = 0$ m s^{-1} constant with height for the whole domain. The roughness length, z_0, is 0.01 m, and the geographic latitude is $\phi = 40^{\circ}$ ($f = 10^{-4}$ s^{-1}). The effects of humidity were not considered in the simulations. Turbulence statistics were calculated every 200 seconds. After approximately one hour of simulation, the simulated flows approximately present an steady state behavior, that is, the TKE does not change significantly with time. The average values, between one and four hours, of the friction and convection velocities, respectively, are 0.73 m s^{-1} and 1.47 m s^{-1} for case W and 0.70 m s^{-1} and 1.33 m s^{-1} for case S.

In order to test the MXL, the evolution of the convective boundary layer was simulated with the mixed layer model using the ZOJ and FOJ approaches and compared against the LES results over a period of 10000 seconds.

2.3 *Initial conditions*

Once the simulated convective boundary layer was well formed, the LES results were used to provide the initial conditions in the ZOJ and the FOJ. Due to the different initial thermal stratification, the formation of a well developed mixed layer can occur at different times, depending on the simulated case. The initial values of h_1, Θ_{vm}, U_m, V_m, $\Delta\Theta_v$, ΔU, ΔV, $\overline{w\theta_v}|_s$, $\overline{wu}|_s$, and $\overline{wv}|_s$ have to be provided to the MXL. Furthermore, in the case of the FOJ, the initial inversion layer thickness must also be specified. Due to the different characterization of the inversion layer in the ZOJ and the FOJ approaches, the definition of the inversion jump values extracted from the LES differ between the ZOJ and FOJ. These jump values are used to initialize and evaluate the ZOJ and the FOJ. Below, we give an exact description of the estimation of each variable:

(a) Boundary layer depth: h_1, height of the minimum virtual potential temperature flux.

(b) Inversion layer thickness: $\delta = h_2 - h_1$, where h_2 is not the height above h_1 defined when the virtual potential temperature flux becomes zero, but when it is larger than 10% of its minimum value. This definition was used because at some specific times the virtual potential temperature flux becomes positive at unrealistic high values of z, especially for case W. However, by using this criterion, h_2 is below the height where the virtual potential temperature flux becomes zero. Therefore, $\delta = h_2 - h_1$ obtained by using this definition is slightly underestimated.

(c) Mean values in the mixed layer: $\Theta_{vm} = \Theta_v(z = h_0/2)$, $U_m = U(z = h_0/2)$, and $V_m = V(z = h_0/2)$, where h_0 is the height below h_1 defined when the virtual potential temperature flux becomes zero (lower crossing).

(d) Temperature jump at the inversion: for this variable, because of the different physical assumptions of the entrainment zone in the ZOJ and the FOJ, two different definitions were used to initialize and compare the MXL results. $\Delta\Theta_{v(FOJ)} = \Theta_v(z = h_2) - \Theta_{vm}$ (Kim et al. 2006), and $\Delta\Theta_{v(ZOJ)} = \Theta_v(z = h_2) - \gamma_\theta(h_2 - h_1) - \Theta_{vm}$ (Fedorovich et al. 2004).

(e) Velocity jumps at the inversion: to keep consistency, these variables are defined in the same way as the temperature inversion jump for ZOJ and FOJ. However, in the cases under study, $\gamma_u = \gamma_v = 0$ s^{-1}, and, therefore, $\Delta U_{ZOJ} = \Delta U_{FOJ}$. Similar definitions are used for ΔV.

(f) Surface momentum fluxes: $\overline{wu}|_s = \overline{wu}(z = 0)$, and $\overline{wv}|_s = \overline{wv}(z = 0)$. The evolution of the surface momentum fluxes for the MXL during 10000 seconds is prescribed based on LES results (not shown here).

Table I summarizes the prescribed initial values of h_1, δ, Θ_{vm}, $\Delta\Theta_v$, U_m, ΔU, V_m, ΔV, and u_* for the ZOJ and the FOJ in the weak and strong inversion cases.

	W	S
h_1 (m)	750	704
δ (m)	250	190
Θ_{vm} (K)	301.75	303.16
$\Delta\Theta_{v(ZOJ)}$ (K)	0.45	1.04
$\Delta\Theta_{v(FOJ)}$ (K)	1.20	2.16
U_m (m s^{-1})	16.50	14.93
ΔU (m s^{-1})	3.50	5.07
V_m(m s^{-1})	0.83	1.85
ΔV (m s^{-1})	-0.83	-1.85
u_* (m s^{-1})	0.742	0.695
w_s (m s^{-1})	0	0

Table 1: Initial values for the mixed layer model simulations of the atmospheric variables obtained from the LES results, where w_s is the subsidence velocity and the definition of the rest of the variables is explained in the text.

3. RESULTS

3.1 *Boundary layer depth and entrainment velocity evolution*

Fig. 1 shows the time evolution of the boundary layer depth and the entrainment velocity simulated with the ZOJ, the FOJ and the LES for the weak inversion case. Fig. 2 shows the evolution of the same variables for the strong inversion case. For the LES, a least squares quadratic fit of the results of the height of the minimum virtual potential temperature flux and of the height of the maximum virtual potential temperature gradient (h_θ) are

carried out in order to avoid the scatter of h_1, which particularly influences to the calculation of the entrainment velocity. As the results show, for both inversion cases h_θ is always higher than h_1.

To study the effect of the other contributions of the TKE equation, in particular the shear production, on the ZOJ results, we carried out an additional run assuming a constant value $\beta = 0.2$ in the ZOJ scheme. As shown in Figs. 1a and 2a, in this latter case the boundary layer depth is clearly underestimated over the whole period of integration by 9% for case W and by 14% for case S. Therefore, for the cases understudy it is necessary to consider at least the shear (productive) contribution to the TKE, which increases the value of the entrainment heat flux, in order to correctly simulate the time evolution of the boundary layer depth by means of a ZOJ.

In order to show the influence of the definition of the velocity scale at the inversion (Kim et al. 2006), we have also included at Figs. 1 and 2 the mixed layer depth and entrainment velocity obtained by the FOJ if the original velocity scale at the inversion ($\Delta\hat{U}$) is prescribed. In the S and W cases, the FOJ parameterization which uses $\Delta\hat{U}$ underestimates LES results.

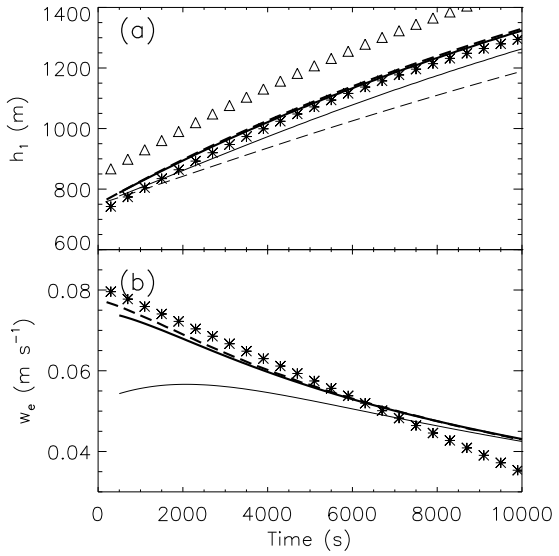

FIG. 1: Time evolution of (a) the boundary layer depth, and (b) the entrainment velocity simulated by means of the LES (asterisks), the ZOJ (thick dashed line), and the FOJ (thick solid line) for the weak inversion case. In (a) the thin dashed line represents the boundary layer depth time evolution simulated by the ZOJ prescribing $\beta = 0.2$ and the thin solid line the boundary layer depth time evolution obtained if the original velocity scale is used in the FOJ (also included in b). In this figure, the triangles show the LES boundary layer depth calculated by means of the height of the maximum virtual potential temperature gradient.

Regarding the comparison between the MXL representations, Figs. 1a shows that both MXL approaches satisfactorily reproduce the values of the boundary layer depth calculated by the LES for case W. If the strong inversion case is considered (Fig. 2a), the ZOJ tends to slightly overestimate, whereas the FOJ underestimates the boundary layer depth obtained by means of the LES.

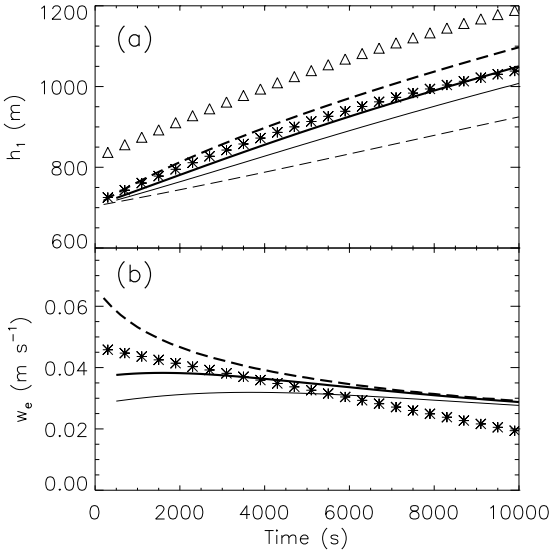

FIG. 2: Same as Fig. 1 for the strong inversion case..

The entrainment velocity is shown in Figs. 1b and 2b. The two MXL approaches approximately follow the evolution of the entrainment velocity obtained by the LES for both CBLs. As shown the FOJ parameterization which uses $\Delta\hat{U}$ leads to lower values compare to LES results. To explain the differences that appear between both MXL, the calculation of the entrainment velocity by the models used in this study is explicitly shown. For the LES, the entrainment velocity is estimated by calculating the time derivative of the least–squares fit of the height of the minimum virtual potential temperature flux:

$$w_{e(LES)} = \left.\frac{\partial h_1}{\partial t}\right|_{(LES)}. \tag{4}$$

In the ZOJ, the entrainment velocity is calculated as follows:

$$w_{e(ZOJ)} = \left.\frac{\partial h_1}{\partial t}\right|_{(ZOJ)} = -\frac{\beta_{ZOJ}}{\Delta\Theta_{v(ZOJ)}}\overline{w\theta_v}|_s, \tag{5}$$

whereas the FOJ calculates the entrainment velocity as (Kim et al. 2006):

$$w_{e(FOJ)} = \left.\frac{\partial h_1}{\partial t}\right|_{(FOJ)} = \frac{\delta - (2h_1 + \delta)\,\beta_{FOJ}}{h_1\left(2\Delta\Theta_{v(FOJ)} - \gamma_\theta\delta\right)}\overline{w\theta_v}|_s, \tag{6}$$

where $\overline{w\theta_v}|_s = 0.1$ K m s^{-1}. As expected, if $\delta = 0$, then $\Delta\Theta_{v(FOJ)} = \Delta\Theta_{v(ZOJ)}$, and (26) reduces to (25).

As occurred for the boundary layer height, both MXL approaches reproduce better the entrainment velocity obtained by means of LES for the case W than for S. By

analyzing the expressions (5) and (6), one can conclude that the discrepancy between the LES and the MXL entrainment velocity occurs because the MXL does not correctly simulate (a) the temperature inversion jump or, (b) the entrainment flux ratio or, (c) in the case of the FOJ, the inversion layer thickness obtained by the LES. If the time evolution of the inversion layer thickness calculated by the FOJ approach and the LES for the two inversion cases is considered (not shown here), one can conclude that the overestimation of the entrainment velocity by FOJ is not caused because of a miscalculation of δ.

3.2 *Mean virtual potential temperature and temperature inversion jump*

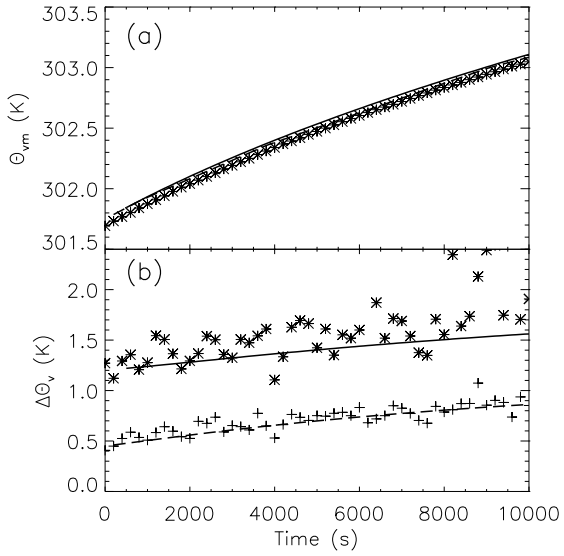

FIG. 3: Time evolution of (a) the mixed layer virtual potential temperature, and (b) the temperature jump at the inversion calculated by means of the LES (symbols), the ZOJ (dashed line), and the FOJ (solid line) for the weak inversion case. Due to the different definition used for $\Delta\Theta_v$ extracted from the LES in order to compare with the ZOJ or the FOJ results, in (b) crosses are used to compare with the ZOJ and asterisks to compare with the FOJ.

The time evolution of the mean virtual potential temperature in the mixed layer, and the temperature inversion jump for cases W and S are shown in Figs. 3 and 4 respectively. The MXL, with the parameterizations (1) and (2), satisfactorily reproduces, with only a slight overestimation, the mean virtual potential temperature evolution obtained with the LES for both case W and case S. Regarding the intercomparison of the temperature inversion jump (Figs. 3b and 4b), the ZOJ reproduces slightly better the LES results than the FOJ for the two inversion cases. As observed, the FOJ, in general, has a tendency to underestimate the temperature inversion jump obtained by the LES.

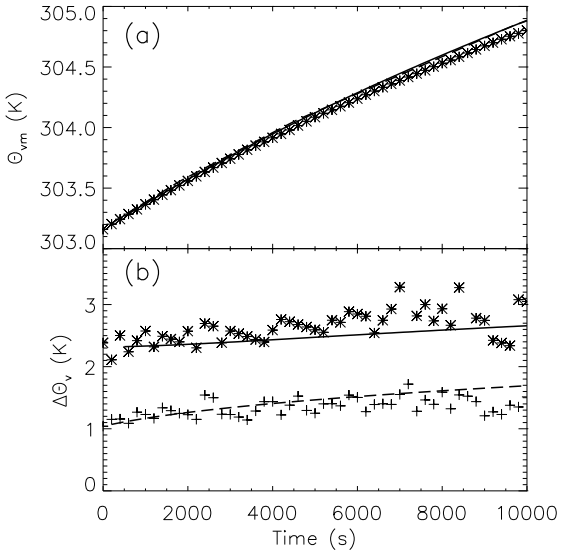

FIG. 4: Same as Fig. 3 for the strong inversion case..

3.3 *Mean wind and velocity inversion jump*

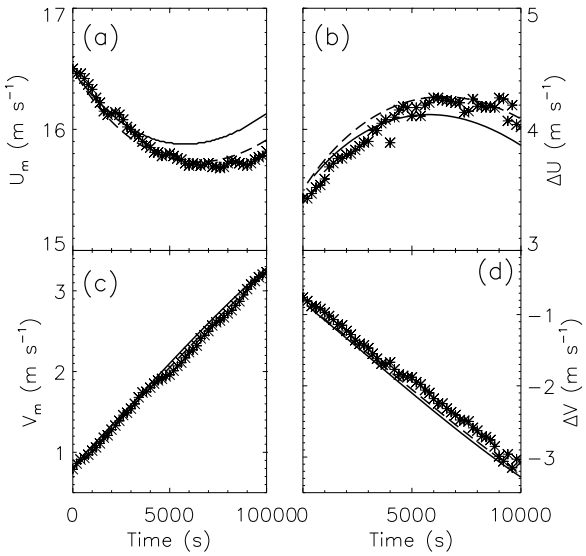

FIG. 5: Time evolution of the two components of the mean wind (left), and their inversion jumps (right): U (top) and V (bottom) calculated by means of the LES (asterisks), the ZOJ (dashed line), and the FOJ (solid line) for the weak inversion case.

Figs. 5 and 6 show, for the weak and strong inversion cases respectively, the mean wind in the mixed layer and the velocity jump at the inversion for the two components of the horizontal velocity. Compared to the LES results, the wind evolution agrees better for case W than for case

S. This fact can be explained by considering, that in the S case, the local effects (shear and dissipation) at the inversion, not considered in the parameterizations of the entrainment fluxes, are potentially more important than in the W case. A possible solution to be tested in the future is to scale shear and dissipation effects with δ. Regarding case W (Fig. 5), the ZOJ agrees better with the LES results than the FOJ for both components of the mean horizontal velocity and inversion jumps. For case S (Fig. 6), the MXL, both ZOJ and FOJ, do not model well the evolution of the wind characteristics. This is particularly evident for U_m (ΔU), which is overestimated (underestimated) by both MXL approaches. The V component is much better simulated by the MXL, especially by the ZOJ. For this case, as showed in Fig. 2b, MXL does not correctly fit the entrainment velocity calculated by means of the LES. Therefore, one can conclude that the entrainment momentum fluxes are also overestimated, and as a consequence the mean velocities in the boundary layer are not correctly reproduced by MXL.

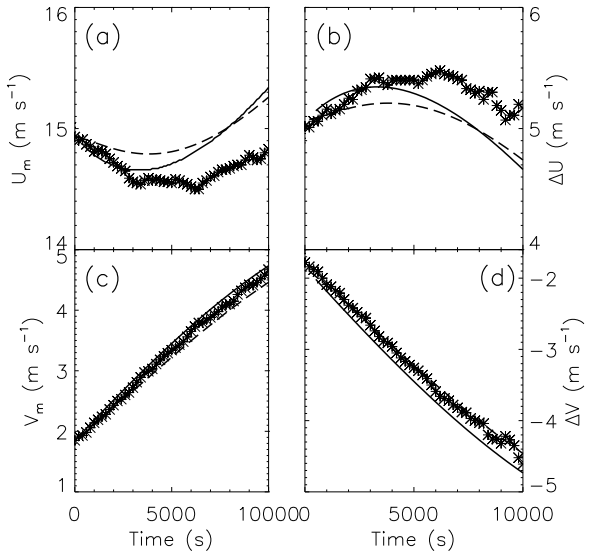

FIG. 6: Same as Fig. 5 for the strong inversion case..

3.4 *Entrainment flux ratio*

Fig. 7 shows the β ratio calculated by means of expression (1) included in the ZOJ, (2) included in the FOJ, and obtained from the LES results by calculating $\beta_{LES} = -\overline{w\theta_v}|_{h_1}(\overline{w\theta_v}|_s)^{-1}$ for the two inversion cases. We have also included β obtained by using $\Delta\hat{U}$ as a reference. By using this definition of $\Delta\hat{U}$, there is a satisfactory agreement between the FOJ and LES results. However, as mentioned previously, these lower β values yields to an underestimation the boundary layer depth and entrainment velocity evolution (see Fig. 1). It is important to notice that, as the same constant surface flux is prescribed for all the models, Fig. 7 only represents the evolution of the virtual potential temperature flux at the entrainment zone.

As shown, both parameterizations included in the MXL overestimate β when compared with the LES results. However, some differences can be observed between the parameterizations of β included in the MXL. β_{ZOJ} gives better results than β_{FOJ} for case W, especially at the beginning of the simulation, when the contribution of the temporal term of the TKE, considered only on the ZOJ description, is relevant.

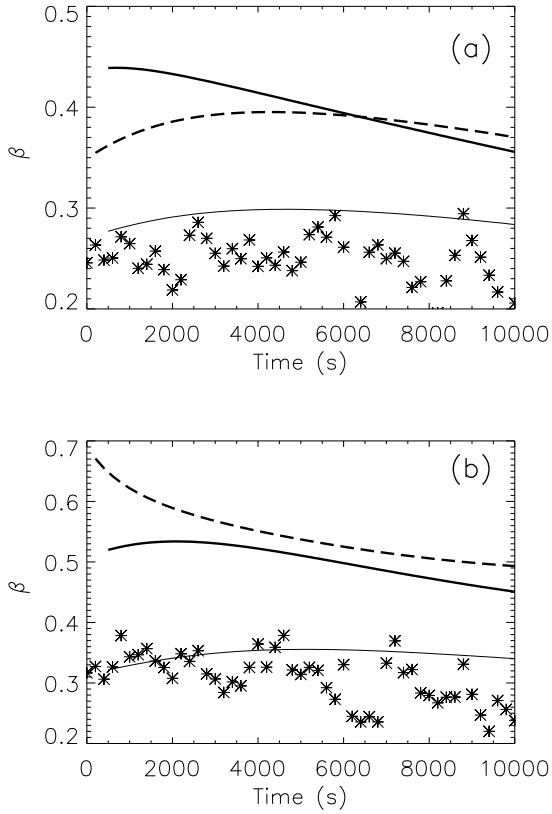

FIG. 7: Time evolution of the ratio between entrainment and surface virtual potential temperature flux, β, obtained for cases (a) W, and (b) S by means of the LES (asterisks), the ZOJ (dashed line), and the FOJ (thick solid line). The thin solid line represents as a reference the time evolution of the entrainment ratio if the original velocity scale at the inversion ($\Delta\hat{U}$) is used.

By contrast, the parameterization included in the FOJ gives better results than those in the ZOJ for case S. In this case, the shear effects are an important contribution to the TKE at the inversion. Furthermore, due to the larger strength of the inversion compared with case W, the local dissipation effects (included in FOJ) might not be negligible.

Another important point in the discussion of the comparison of the entrainment fluxes between LES and MXL, and two of the assumptions used to derive (1) and (2),

are the possible reasons for the overestimation: (a) the MXL, which explicitly assumes that the virtual potential temperature flux is linear profile up to h_1, always results in higher entrainment heat flux values than those obtained from the equivalent simulated LES profile. In the studied cases, this approximation produces values of the virtual potential temperature flux at the inversion 1.5 times larger than the LES value; (b) as Lilly (2002a) pointed out, LES entrainment fluxes are smoothed due to the horizontal average of the large–scale fluctuations at the mixed layer top. Therefore, LES results produce always smaller results of the minimum virtual potential temperature flux when comparing with mixed layer model; and (c) this may be further enhanced by the mathematical form of expressions (1) and (2), which include the elevated shear effect with a negative sign in the denominator. It was expected that the inclusion of the of other terms, not considered in β_{ZOJ} (non–local dissipation effects) or β_{FOJ} (time tendency of the TKE), would control the contribution of the shear to the entrainment flux during the simulation.

3.5 *Virtual potential temperature flux partitioning*

By observing Fig. 7 one may wrongly conclude that, especially for case S, that the MXL does not accurately simulate the amount of heat entrained in the boundary layer. In order to further study this point, we apply another method to evaluate the calculation of the entrainment heat flux. The flux partitioning method divides the virtual potential temperature flux into a TKE consuming part and a TKE producing part. We compare the ratio between these parts obtained from the LES and the MXL. Here, we use the Eulerian partitioning of the flux. the positive (P) and negative (N) parts of the total integral of the virtual potential temperature flux are defined as follows:

$$N = \int_0^{h_2} (\overline{w\theta_v} < 0) dz, \quad P = \int_0^{h_2} (\overline{w\theta_v} > 0) dz. \quad (7)$$

In this section, the ratio $A = -NP^{-1}$ is calculated for the MXL, and compared against the LES results. In the case of the MXL, P and N depend on the values of h_1, β, $h_0 = h_1(1+\beta)^{-1}$, and δ. It is straightforward to show that the ratio reads:

$$A = \beta \left[\beta + \frac{\delta}{h_1} (1+\beta) \right], \quad (8)$$

where β is calculated by means of (1) for ZOJ ($\delta = 0$), or by using (2) in the case of FOJ.

Fig. 8 shows the time evolution of A obtained by using (8) for the MXL, and integrating the LES virtual potential temperature flux profile during the CBL evolution for the two inversion cases. The large scatter obtained in the LES results is partly due to the fluctuations of h_0, and of h_2 in particular. Because the same surface fluxes are defined for the MXL and the LES, P only depends on the value of h_0 obtained for each model. For the two cases studied, MXL fits well the area of positive virtual potential temperature flux obtained by means of the LES (not shown here). Therefore, the differences between MXL and LES observed in Fig. 8 are only because the MXL is only able to reproduce partially the values of N obtained by means of the LES.

Regarding case W (large δ), as shown in Fig. 8a, the ZOJ underestimates, whereas the FOJ overestimates A obtained by means of the LES. The ZOJ approach, which overestimates β (Fig. 7a), produces lower values of A than the LES due to the assumption $\delta = 0$. In this case, the δ simulated values by means of LES (not shown here) are far from the ZOJ assumption. Conversely, the FOJ approach, which fits the LES δ time evolution (not shown here) but overestimates the absolute value of the minimum of the virtual potential temperature flux (Fig. 7a), also overestimates A, as was expected.

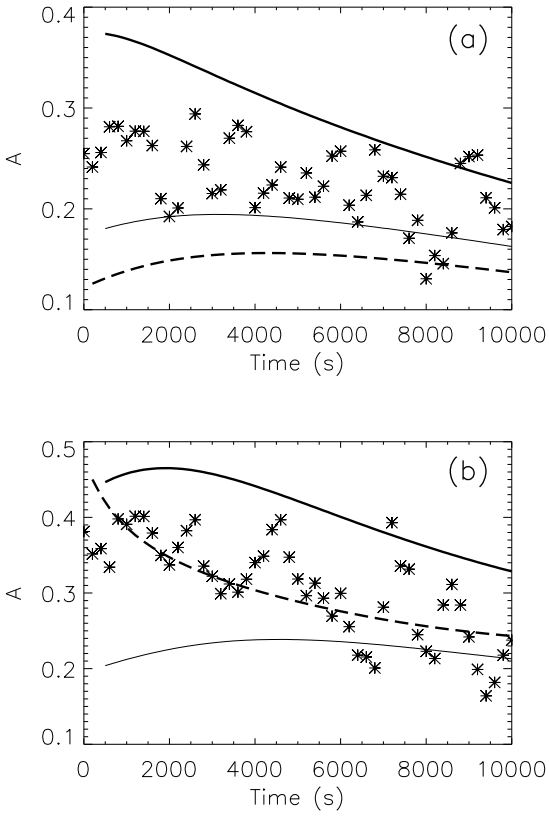

FIG. 8: Time evolution of the ratio between the integral of the negative and positive parts of the virtual potential temperature flux, obtained for cases (a) W, and (b) S by means of the LES (asterisks), the ZOJ (dashed line), and the FOJ (solid line).The thin solid line represents as a reference the time evolution of the ratio if the original velocity scale at the inversion ($\Delta\hat{U}$) is used.

If case S is analyzed (Fig. 8b), the FOJ overestimates the value of A obtained by means of the LES for same reasons explained above. Conversely, for this case, the ZOJ fits quite well A obtained by the LES. If a strong inversion strength is considered, δ is lower than for case W. Therefore, for this case, the assumption $\delta = 0$ pre-

scribed in the ZOJ is approximately compensated by the overestimation of the minimum virtual potential temperature flux, and the ZOJ correctly reproduces the value of A obtained by the LES.

From the analysis of the results, we suggest that an intercomparison of different entrainment flux parameterizations against the LES results cannot only be based on the value of the minimum of the virtual potential temperature flux obtained for each parameterization. In our opinion, the use of the Eulerian, or process heat flux partitioning is a more suitable method since it takes better into account the regions dominated by the positive heat flux, driven by the surface fluxes, and the negative heat flux (entrainment).

4. CONCLUSIONS

In order to quantitatively further analyze and summarize the differences between the LES and the mixed layer model, the root mean square error ($rmse$) and the root mean square vector error ($rmsve$) were used. These statistical estimators are defined in our study as follows:

$$rmse_{MXL} = \left[\frac{\sum_{i=1}^{n} \left(\Phi^i_{MXL} - \Phi^i_{LES} \right)^2}{n} \right]^{1/2}, \quad (9)$$

$$rmsve_{MXL} = \left\{ n^{-1} \sum_{i=1}^{n} \left[\left(\Psi^i_{MXL} - \Psi^i_{LES} \right)^2 + \left(\Pi^i_{MXL} - \Pi^i_{LES} \right)^2 \right] \right\}^{1/2}, \quad (10)$$

where Φ is a scalar variable, in our case h_1, δ, w_e, β, A, Θ_{vm} or $\Delta\Theta_v$. Ψ and Π refer to each wind component, or their respective inversion jumps, n is the total number of times simulated, and subscript MXL refers either to the mixed layer model using the ZOJ or the FOJ parameterizations. The ZOJ and the LES results are written every 200 seconds, whereas the FOJ writes its output every 100 seconds. Between $t = 0$ and $t = 10000$ seconds, the number of incidences of simultaneous output is $n = 48$.

Table 2 shows the $rmse$ or $rmsve$ of the ZOJ and the FOJ for each variable and for cases W and S. Regarding case W, the ZOJ and the FOJ give similar values of the $rmse$ for most of the considered variables. The high value obtained for δ, and $\Delta\Theta_v$ in the case of the FOJ is partially attributed to the scatter of the determination of h_2 from the LES results, especially in case W. Only if the $rmsve$ of the velocities and their inversion jumps are considered, one can conclude that the ZOJ simulates the the wind components and their inversion jumps better than the FOJ. The same results are obtained for case S. For this case, though the ZOJ overestimates U_m more than the FOJ, the obtained $rmsve$, which includes the two components of the horizontal velocity, is slightly lower than the one obtained with the FOJ. A similar result is obtained when one analyzes the inversion jump of the velocities. In summary, Table 2 shows that the ZOJ fits the LES results better.

	W		S	
	ZOJ	FOJ	ZOJ	FOJ
h_1 (m)	23.1	18.5	31.4	14.9
δ (m)	–	106	–	60
β	0.141	0.157	0.238	0.197
A	0.086	0.081	0.047	0.112
w_e (m s^{-1})	0.0033	0.0038	0.006	0.005
Θ_{vm} (K)	0.039	0.061	0.047	0.048
$\Delta\Theta_v$ (K)	0.076	0.373	0.19	0.39
M (m s^{-1})	0.081	0.609	0.31	0.65
ΔM (m s^{-1})	0.16	0.52	0.26	0.58

Table 2: Root mean square error or root mean square vector error of the ZOJ and the FOJ for each of the analyzed variables. M and ΔM represents, respectively, the $rmsve$ of the two components of horizontal wind velocity, and their respective inversion jumps.

We have shown that the FOJ and the ZOJ approaches produce similar results for the two inversion cases. The mixed layer model results agree well with the boundary layer depth, mixed layer variables and inversion jumps obtained from the LES, with a better agreement in the case of weak inversion. If the two MXL approaches are compared, one would expect that, as δ increases (weak inversion), the FOJ ($\delta \neq 0$) would better fit the LES data than the ZOJ does. For the cases studied, and considering the mixed layer variables, this was not observed.

Regarding the entrainment velocity, both MXL approximately reproduce the LES values with a slight overestimation for the case with a strong inversion. Due to the definitions of the entrainment velocity used in the MXL and the good agreement obtained by the MXL for $\Delta\Theta_v$ and δ (not shown here), the differences in w_e between MXL and LES are caused because MXL overestimates β obtained by means of LES. One possible explanation for the disagreement in β is based on the linear profile of the virtual potential temperature flux from the surface up to h_1 assumed by the MXL. This approximation always results in higher values of the entrainment heat flux for the MXL compared to the LES results. A second reason is related to the smoothing effect of horizontal averaging, which reduces the value of the entrainment heat flux obtained by LES. Finally, the contribution of the shear to the entrainment heat flux could be overstated in the MXL, especially for the ZOJ approach. In the FOJ, the inclusion of the non–local dissipation effects explicitly in (2) reduces the shear contribution to the TKE. This can be more clearly observed in cases with a strong inversion (case S).

The entrainment heat flux parameterizations included in the MXL have also been studied by using Eulerian heat flux partitioning. For this variable, LES and MXL results agree more closely than they do if the ratio of the entrainment flux to the surface flux is used as the basis for comparison, especially for the ZOJ. In our opinion, the comparison only using the single values of the virtual potential temperature flux could lead to mislead-

ing results. The heat flux partitioning method is more appropriate since it accounts for the distribution of the heat in the whole boundary layer. For this reason, we suggest that in any entrainment parameterization intercomparison, besides the comparison of β itself, the comparison of the heat flux partitioning has to be considered in order to analyze the performance of each parameterization.

The agreement obtained for the boundary layer depth (h_1) and mixed layer variables (Θ_{vm}, U_m and V_m) is particularly encouraging, because these variables are fundamental for describing the diurnal variability of the boundary layer in Global Circulation and Chemistry Transport Models. The results show that both parameterizations of the entrainment flux (the ZOJ and the FOJ) provide an accurate description of it as a function of the relevant processes that drive this flux at the interface between the boundary layer and the free troposphere.

Acknowledgments

This work was supported by the visiting study program of KOSEF (Korea Science and Engineering Foundations), NCAR visiting scientist program, the Stichting Nationale Computerfaciliteiten (National Computing Facilities Foundation, NCF) with the project SG-132 for the use of supercomputing facilities, with financial support from the Netherlandse Organisatie voor Wetenschappelijk Onderzoek (Netherlands Organization for Scientific Research, NWO) and Spanish MCYT scientific project REN2003–03436. J. Vilà was partially supported during his visit to NCAR by the NWO project R76–241.

REFERENCES

Betts, A. K., 1973: Non–precipitating cumulus convection and its parameterization. *Quart. J. Roy. Meteor. Soc.*, **99,** 178–196.

Cuijpers, J. W. M., and P. G. Duynkerke, 1993: Large eddy simulation of trade wind cumulus clouds. *J. Atmos. Sci.*, **50,** 3894–3908.

——, and A. A. M. Holtslag, 1998: Impact of skewness and nonlocal effect on scalar and buoyancy fluxes in convective boundary layers. *J. Atmos. Sci.*, **55,** 151–162.

Deardorff, J. W., G. E. Willis, and B. H. Stockton, 1980: Laboratory studies of the entrainment zone of a convectively mixed layer. *J. Fluid Mech.*, **100,** 41–64.

Fedorovich, E., R. Conzemius, and D. Mironov, 2004: Convective entrainment into a shear–free, linearly stratified atmosphere: Bulk models reevaluated through large eddy simulations. *J. Atmos. Sci.*, **61,** 281–295.

Garratt, J. R., 1992: *The Atmospheric Boundary Layer*. Cambridge University Press, Cambridge, 316 pp.

Kim, S. –W., S. –U. Park, D. Pino, and J. Vilà–Guerau de Arellano, 2006: Entrainment parameterization in a sheared convective boundary layer by using a first–order jump model. *Bound.–Layer Meteor.* In press.

Lilly, D. K., 1968: Models of cloud–topped mixed layer under a strong inversion. *Quart. J. Roy. Meteor. Soc.*, **94,** 292–309.

——, 2002a: Entrainment into mixed layers. Part I: Sharp–edged and smoothed tops. *J. Atmos. Sci.*, **59,** 3340–3352.

——, 2002b: Entrainment into mixed layers. Part II: A new closure. *J. Atmos. Sci.*, **59,** 3353–3361.

Mahrt, L., and D. H. Lenschow, 1976: Growth dynamics of the convectively mixed layer. *J. Atmos. Sci.*, **33,** 41–51.

Pino, D., J. Vilà–Guerau de Arellano, and P. G. Duynkerke, 2003: The contribution of shear to the evolution of a convective boundary layer. *J. Atmos Sci.*, **60,** 1913–1926.

Sorbjan, Z., 2004: Large–eddy simulations of the baroclinic mixed layer. *Bound.–Layer Meteor.*, **112,** 57–80.

Stull, R. B., 1976a: The energetics of entrainment across a density interface. *J. Atmos. Sci.*, **33,** 1260–1267.

——, 1976b: Mixed–layer depth model based on turbulent energetics. *J. Atmos. Sci.*, **33,** 1268–1278.

——, 1988: *An Introduction to Boundary Layer Meteorology*. Kluwer Academic Press, Dordrecht, 670 pp.

Tennekes, H., 1973: A model for the dynamics of the inversion above a convective boundary layer. *J. Atmos. Sci.*, **30,** 558–567.

——, and A. G. M. Driedonks, 1981: Basic entrainment equations for the atmospheric boundary layer. *Bound.–Layer Meteor.*, **20,** 515–531.

Zeman, O., and H. Tennekes, 1977: Parameterization of the turbulent energy budget at the top of the daytime atmospheric boundary layer. *J. Atmos. Sci.*, **34,** 111–123.